Science of the Total Environment 923 (2024) 171438

Contents lists available at ScienceDirect

Science of the Total Environment

journal homepage: www.elsevier.com/locate/scitotenv

Selective recovery of boron, cobalt, gallium and germanium from seawater solar saltworks brines using *N*-methylglucamine sorbents: Column operation performance

V. Vallès [a,b,*], M. Fernández de Labastida [a,b], J. López [a,b], J.L. Cortina [a,b,c]

[a] Chemical Engineering Department, Escola d'Enginyeria de Barcelona Est (EEBE), Universitat Politècnica de Catalunya (UPC)-BarcelonaTECH, C/Eduard Maristany 16, Campus Diagonal-Besòs, 08019 Barcelona, Spain
[b] Barcelona Research Center for Multiscale Science and Engineering, C/Eduard Maristany 16, Campus Diagonal-Besòs, 08019 Barcelona, Spain
[c] CETaqua, Carretera d'Esplugues, 75, 08940 Cornellà de Llobregat, Spain

HIGHLIGHTS

- Need for alternative sustainable sources for critical raw materials (e.g. B)
- Waste brines from saltworks as an alternative sustainable resource
- *N*-methylglucamine sorbents to recover selectively B, Co, Ga and Ge from brines
- Concentration factors up to 11 for B after elution with 1 M HCl
- Mass transfer modelling to describe the extraction of trace elements

GRAPHICAL ABSTRACT

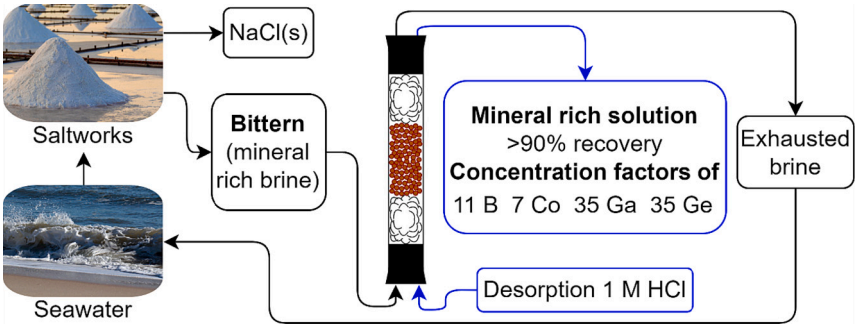

ARTICLE INFO

Editor: Damià Barceló

Keywords:
Boron
Gallium
Germanium
Chelating sorbent
Brine
Ion exchange

ABSTRACT

The European Union (EU) identified a list of Critical Raw Materials (CRMs) crucial for its economy, aiming to find alternative sources. Seawater is a promising option as it contains almost all elements, although most at low concentrations. However, to the present, the CRMs' recovery from seawater is technically and economically unfeasible. Other alternatives to implement sea mining might be preferred, such as reverse osmosis brines or saltworks bitterns (after sodium chloride crystallisation). The CRMs' extraction in a selective way can be achieved using highly selective recovery processes, such as chelating sorbents. This study focuses on extracting Trace Elements (TEs) from solar saltworks brines, including boron, cobalt, gallium and germanium, using commercial *N*-methylglucamine sorbents (S108, CRB03, CRB05). The application of these sorbents has shown potential for boron recovery, but their selectivity for cobalt, gallium, and germanium requires further investigation. This research aims to assess these sorbents' kinetics and column mode performance for TEs recovery from synthetic bitterns. Boron and germanium were rapidly sorbed, reaching equilibrium (>90 %) within 1 h, except for S108, which took 2 h. In column mode, 20–25 pore volumes of bittern were treated to remove boron and germanium, but competition from other elements reduced treatment capacity. An acidic elution (1 M hydrochloric acid)

* Corresponding author at: Chemical Engineering Department, Escola d'Enginyeria de Barcelona Est (EEBE), Universitat Politècnica de Catalunya (UPC)-BarcelonaTECH, C/Eduard Maristany 16, Campus Diagonal-Besòs, 08019 Barcelona, Spain.
E-mail address: victor.valles.nebot@upc.edu (V. Vallès).

https://doi.org/10.1016/j.scitotenv.2024.171438
Received 24 January 2024; Received in revised form 29 February 2024; Accepted 1 March 2024
Available online 2 March 2024

allowed to elute them (>90 %), reaching concentration factors for germanium and boron of 35 and 11, respectively, while cobalt and gallium had less affinity for the sorbents. In addition, the experiments performed were fitted by a mass transfer model to determine the equilibrium constants and selectivities. Therefore, bittern mining has been proven as a secondary/alternative source to obtain CRMs, which can lead the EU to a position in which its dependence on other countries to obtain these raw materials would be decreased.

1. Introduction

European Union (EU) created, in 2011, a list where 14 elements and minerals were included and recognised as Critical Raw Materials (CRMs) considering their supply risk and their economic importance for the EU. Over the past years, this list has been reviewed, and nowadays, it includes up to 34 CRMs (European Commission, 2023). Moreover, in 2023 the EU adopted the term "strategic raw material" because of the importance of some elements for strategic sectors, whose demand is expected to grow in the following years. In both lists, elements such as boron (B), gallium (Ga) and germanium (Ge) are included (European Commission et al., 2023). For that reason, the EU is promoting circular economy models that will provide new alternative sources for these elements or minerals, avoiding, therefore, the dependence on external countries. Similarly, the United States (US) Geological Survey launched in 2020 a list of critical minerals, and it was updated in 2022, including also Ga and Ge among them (Burton, 2022).

Seawater has been considered one of the best alternative sources to recover critical elements based on the concept of sea mining, as seawater contains almost every single element of the periodic table (Kumar et al., 2021; Quist-Jensen et al., 2016), although most of them at concentrations lower than mg/L levels, and in some cases at μg/L (Zhang et al., 2021). Nowadays, it has been demonstrated that some of the seawater's most concentrated components, such as sodium (Na), potassium (K) or magnesium (Mg), are already feasible to extract (Jeppesen et al., 2009; Bardi, 2010; Shahmansouri et al., 2015). However, those at mg/L levels or lower, namely Trace Elements (TEs), are not plausible to extract, as the extraction process will be energy-intensive (Bardi, 2010; Pramanik et al., 2020). Bardi (2010) calculated that $2{\cdot}10^8$ TWh would be required to obtain the yearly copper production from seawater, being four orders of magnitude higher than the yearly electric energy production. In addition, the economic viability of extracting minerals from seawater or desalination brines (with double the seawater concentration (Shahmansouri et al., 2015)) has been determined by several researchers (Kumar et al., 2021; Shahmansouri et al., 2015; Loganathan et al., 2017; Sharkh et al., 2022). In addition, based on the seawater concentration and their market prices, the economic feasibility of extracting minerals from direct seawater is presented in Fig. S1. Most of the minerals economically challenging to be extracted from seawater are so due to their extremely low concentration (below 1 mg/L). Therefore, their extraction would require a concentration step using thermal technologies, such as multi-stage flash, which consumes about 80–120 kWh per m^3 of water treated (Thabit et al., 2022).

Nevertheless, other routes can be explored taking benefit from concentrated brines. In that way, the EU is funding research projects based on sea mining (CORDIS, 2021a, 2021b) that aim to recover several raw materials (either critical or not) from different types of brines, either from desalination plants or from seawater solar saltworks. In the last case, the origin of the brine takes place in saltworks, which are defined as extended areas in which seawater feeds a group of shallow ponds where, then, seawater is evaporated and concentrated by solar and wind action causing sea salt (sodium chloride, NaCl) crystallisation (Davis, 2018; Gorjian et al., 2019). Once the salt is crystallised, the remaining liquid, called *bittern*, is 20 to 40 times more concentrated than seawater in certain elements and, in addition, it has a low content of calcium (Ca) (mainly <0.2 g/L (Randazzo et al., 2024)). As example, the characterisation of the bittern along the saltworks ponds in Trapani (Italy) found out an increase in B concentration from 4.5 mg/L (in seawater) to 79 mg/L (in the bittern, after NaCl crystallisation) (Vicari et al., 2022). In the saltworks, these bitterns are normally considered and managed as waste. However, their higher concentration compared to seawater can make feasible a recovery process, and recently, it was estimated that it can be possible to produce up to 4441 t of boron oxide (B_2O_3(s)) per year in the Euro-Mediterranean area (Randazzo et al., 2024). Therefore, the extraction of B from bitterns could be a potential alternative source, given that 98 % of European demand for B is supplied, in the form of borates, by Turkey (European Commission, 2020).

According to literature (Simonnot et al., 2000; Nasef et al., 2014; Wolska and Bryjak, 2013), several methods could be used to recover B from aqueous saline solutions, such as precipitation-coagulation, evaporation-crystallisation, solvent extraction or membrane filtration after complexation, reverse osmosis (RO), electrodialysis (ED) and ion exchange (IX). However, B removal is not highly efficient when employing coagulation and chemical precipitation, and methods like evaporation-crystallisation or solvent extraction are most appropriate for solutions with a high content of B (Cyganowski et al., 2021). In addition, most of these technologies present relevant disadvantages regarding the B recovery due to the intensive use of chemicals and the cost associated with their use and operation. Apart from that, depending on the pH of the solution, B can be found as boric acid (H_3BO_3) ($pK_{a,298K}$ (H_3BO_3/borate ($H_2BO_3^-$)) = 8.8), which can make difficult its separation when using membrane technologies (Nasef et al., 2014). As an alternative, chelating sorbents, especially those based on *N*-methylglucamine functional groups, have proven to be an effective method for B recovery from aqueous streams (Guan et al., 2016; Kabay et al., 2007; Kabay et al., 2010; Çermikli et al., 2020). These chelating sorbents have higher selectivity than conventional IX sorbents and can be easily regenerated at not so concentrated acidic pH values (Hubicki and Kołodyńska, 2012). Nowadays, some of them are commercialised, such as the Amberlite IRA743, Purolite S108 and Diaion CRB03 and CRB05, aiming to remove B from potable water. Some studies (Şen et al., 2021; Çermikli et al., 2023) have proven that hybrid methods, combining RO and IX with this type of chelating sorbents were able to remove B from geothermal waters containing around 10 mg/L of B.

Nevertheless, the performance of *N*-methylglucamine sorbents has been also studied when applied for brines (Melnyk et al., 2005; Nishihama et al., 2013; Figueira et al., 2022). Melnyk et al. (2005) have stated that, regardless of the experimental conditions, the B removal efficiency of *N*-methylglucamine sorbents ranges normally between 93 % and 98 %. Nishihama et al. (2013) studied the B adsorption on Diaion CRB03 and CRB05 sorbents and on Chelest Fiber GRY-HW (all of them containing the *N*-methylglucamine functional group) in batch mode (2 $g_{sorbent}$/L) varying the concentration of pure B solution from around 10 to 250 mg/L at a pH of 6.05–6.30. They reported Langmuir's maximum adsorption capacities for B of 10.7, 12.7, and 12.4 mg/g for CRB03, CRB05, and Chelest Fiber, respectively. In that study, it was also studied the removal of B from pure B solutions (800 mg/L) in column operation using the best two sorbents, the CRB05 and the Chelest Fiber. They concluded that the fiber sorbent in the column presented higher capacity, requiring 10 Bed Volumes (BV) in front of the 7 BV needed for CRB05. Then, that sorbent was evaluated using a single component B solution and a salt lake brine, showing similar performance in terms of recovery (99.5 % for the single-component solution and 82 % for the brine). Recently, Figueira et al. (2022) evaluated three *N*-methylglucamine sorbents (Purolite S108 and Diaion CRB03 and CRB05) for B recovery from seawater RO brines. Initially, the authors have

characterised the sorbents in terms of isotherms and kinetics experiments, observing that CRB03 presented the highest Langmuir maximum sorption capacity (16.6 mg/g) in front of S108 (10.9 mg/g) and CRB05 (12.9 mg/g), all of them evaluated at pH 5.9. Thus, this sorbent was selected to be evaluated under column mode, using a single-component B solution of 50 mg/L. As a result, they reported a sorption capacity for B of 12.9 mg/g and a 98 % recovery after desorbing it with 4 % hydrochloric acid (HCl), which led to a B concentration factor of 30. Even though the applicability of *N*-methylglucamine to recover B from brines is widely studied, the literature is scarce on its application to solar saltworks bitterns. Recently, Vallès et al. (2023a) evaluated under batch mode different types of sorbents differing on their functional groups to target TEs, showing that the *N*-methylglucamine sorbents are useful for B recovery, but also for targeting Ga, Ge and cobalt (Co). However, no column experiments were conducted. Therefore, despite the research carried out with brines, there is still a significant lack of studies considering bitterns as a source for the recovery of CRMs. For this reason, and considering the potential of such naturally concentrated brines (up to 40 times compared to seawater), which are also normally considered waste, this paper aims to fill this research gap. The main new contributions of the research carried out in this work are related to the development of mineral recovery schemes from bitterns.

This work evaluated three *N*-methylglucamine sorbents (Purolite S108, Diaion CRB03 and CRB05) to recover B from solar saltworks bitterns under column mode operation. Initially, the sorption kinetics were evaluated to assess the residence time required inside the column to reach equilibrium, and therefore the inlet flowrate. Then, the sorbents were evaluated under different experimental conditions in terms of salinity to determine the breakthrough curves. Following saturation, the sorbents were regenerated using 1 M HCl and the elution profiles were also determined. A multi-component mass transfer model was used to describe the batch kinetic profiles, the breakthrough and elution curves in the column experiments, and the sorbents' selectivity coefficients. Results on column operation were compared in terms of sorbent capacity, concentration factor and recovery ratio. The behaviour of major (B, Ca, Mg, Na, sulphate (S) and K) and minor components (lithium (Li), rubidium (Rb), caesium (Cs), strontium (Sr), Ga, Ge and Co) was also evaluated along the sorption and desorption stages.

2. Materials and methods

2.1. Chemicals

The sorption stage of the experiments was performed with synthetic solutions, whereas desorption was performed with 1 M HCl. The chemicals used for preparing those solutions were: NaCl (>99.9 %, Glentham LIFE SCIENCES), potassium chloride (KCl, >99 %, Sigma-Aldrich), magnesium chloride hexahydrate ($MgCl_2{\cdot}6H_2O$, >99 %, Sigma-Aldrich), calcium dihydrate ($CaCl_2{\cdot}2H_2O$, 98 %, Sigma-Aldrich), lithium chloride (LiCl, >99 %, Sigma-Aldrich), H_3BO_3 (>99.5 %, Sigma-Aldrich), cobalt chloride hexahydrate ($CoCl_2{\cdot}6H_2O$, >98 %, Alfa Aesar), rubidium carbonate (Rb_2CO_3, 99 %, Sigma-Aldrich), strontium chloride hexahydrate ($SrCl_2{\cdot}6H_2O$, >98 %, Alfa Aesar), caesium chloride (CsCl, >99.9 %, Glentham LIFE SCIENCES), sodium sulphate anhydrous (Na_2SO_4, >99.5 %, Glentham LIFE SCIENCES), sodium bromide (NaBr, >99 %, Sigma-Aldrich), HCl (37 %, Sigma-Aldrich), sodium hydroxide (NaOH, >97 %, Glentham LIFE SCIENCES), Ge plasma standard solution (10,000 mg/L, Alfa Aesar) and Ga plasma standard solution (10,000 mg/L, Alfa Aesar). Sodium carbonate (Na_2CO_3, 99.5 % PanReac), sodium hydrogen carbonate ($NaHCO_3$, 99.5 %, PanReac) and nitric acid (HNO_3, 69 %, PanReac) were used for analytical purposes.

2.2. Chelating sorbents

This study evaluated three different chelating sorbents with *N*-methylglucamine functional groups (Purolite S108, Diaion CRB03 and Diaion CRB05) in column mode experiments. As indicated in the literature (Virolainen et al., 2013), this type of sorbent is known to have a high affinity to capture B. A summary of their main properties is collected in Table S1 (Mitsubishi Chemical, 2007, 2011; Purolite, 2020).

The conditioning of the sorbents was performed by agitating the sorbents for 1 h under magnetically stirring with 1 M NaOH in a solid/liquid ratio of 20 g/L. Then, the sorbents were washed several times with deionised water until achieving a neutral pH value to displace the excess of NaOH used.

2.3. Solution composition

The SEArcularMINE project (SEArcularMINE, 2020), one of the EU's funded projects, is based on the recovery of CRMs, being focused on Mg, Li, Sr, Cs, Rb, Co, Ga, Ge and B. Within the project, it is expected that several core and auxiliary technologies will be integrated aiming to recover selectively each of the above-mentioned elements. According to the process outline, the *bittern* is expected to be firstly treated to recover magnesium hydroxide ($Mg(OH)_2(s)$) (Romano et al., 2023; Battaglia et al., 2023), following a pre-concentration step, being later focused on the Li and TEs recovery (including B, Co, Ga and Ge, among others) (Vallès et al., 2023a; Saif et al., 2021; Saif et al., 2023; Vallès et al., 2023b), as shown in Fig. 1. Finally, the exhausted brine will be used to produce NaOH and HCl using electrodialysis with bipolar membranes (EDBM), which will enhance the circularity of the process (León et al., 2022; Filingeri et al., 2023).

Therefore, according to the efficiency of these previous stages (pre-treatment in Fig. 1), several synthetic bitterns were prepared mimicking the solution expected to be treated with chelating sorbents.

The following synthetic bitterns (composition shown in Fig. 1) were prepared. Major elements are considered the ones in g/L and minor elements or TEs the ones in mg/L or lower.

- Bittern 1: B is expected to be recovered at the TEs-unit, after several pre-treatment stages, including Mg and Li recovery.
- Bittern 2: B is expected to be recovered at the TEs-unit after several pre-treatment stages, including Mg and Li recovery. Higher removals of Ca and Mg are expected compared to bittern 1, as reported by Vassallo et al. (2021).
- Bittern 3: B is expected to be recovered as the first step of the circular process suggested by SEArcularMINE to avoid the presence of boron impurities on the $Mg(OH)_2$ obtained (Robinson et al., 1943; Maskal et al., 1966). Then, as no pre-treatment would be required, Mg is expected to be found in high concentration (38 g/L).

2.4. Kinetics performance

Firstly, kinetic batch experiments were performed by putting in contact for 24 h under magnetically stirring an amount of dry conditioned sorbents with the bittern 1 in a solid/liquid ratio of 30 $g_{sorbent}/L_{bittern}$. Samples were taken at 10, 20, and 30 min and then every hour for 9 h. After 24 h, another sample was taken before finishing the test. The pH was monitored and the samples were analysed by Inductively Coupled Plasma Optical Emission Spectroscopy (ICP-OES) and Mass Spectroscopy (ICP-MS).

The sorption of the elements was calculated as shown in Eq. (1) (Figueira et al., 2022).

$$Sorption = 100\%{\cdot}\frac{C_0 - C_t}{C_0} \quad (1)$$

where C_t and C_0 are the target element measured concentration in the bittern (mg/L or μg/L) at time t and at the beginning of the experiment, respectively.

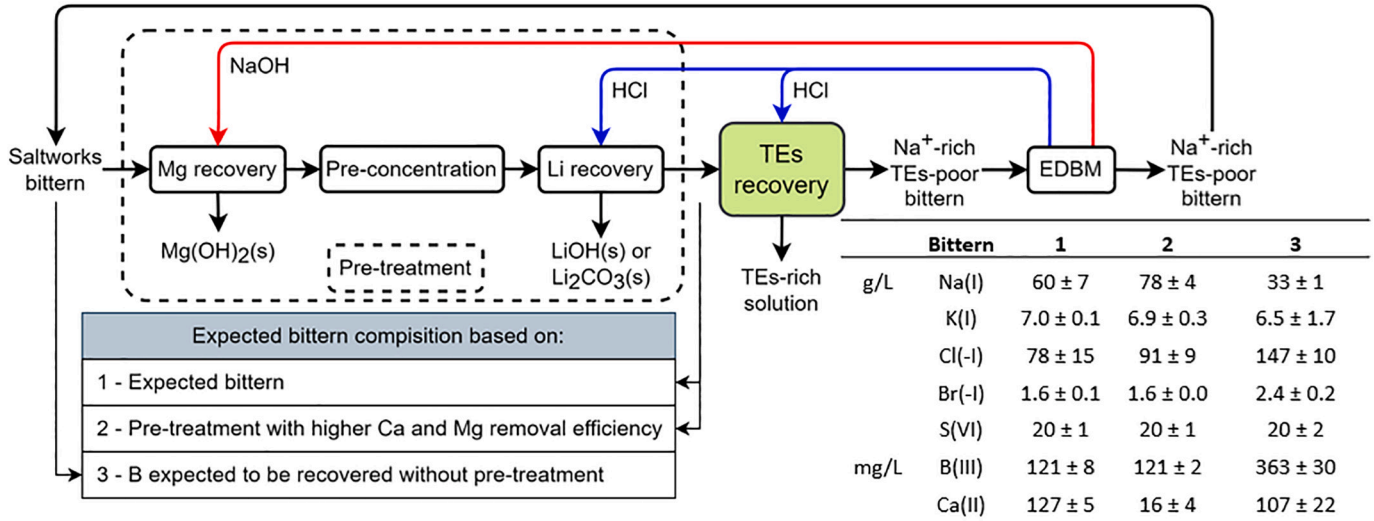

	Bittern	1	2	3
g/L	Na(I)	60 ± 7	78 ± 4	33 ± 1
	K(I)	7.0 ± 0.1	6.9 ± 0.3	6.5 ± 1.7
	Cl(-I)	78 ± 15	91 ± 9	147 ± 10
	Br(-I)	1.6 ± 0.1	1.6 ± 0.0	2.4 ± 0.2
	S(VI)	20 ± 1	20 ± 1	20 ± 2
mg/L	B(III)	121 ± 8	121 ± 2	363 ± 30
	Ca(II)	127 ± 5	16 ± 4	107 ± 22
	Mg(II)	387 ± 18	10 ± 1	38000 ± 7000
	Rb(I)	4.2 ± 0.1	4.1 ± 0.3	2.5 ± 0.5
	Sr(II)	9.2 ± 0.6	3.4 ± 0.1	0.4 ± 0.1
	Li(I)	2.9 ± 0.1	0.3 ± 0.0	282 ± 78
µg/L	Co(II)	282 ± 21	295 ± 37	231 ± 2
	Ga(III)	278 ± 47	259 ± 34	236 ± 61
	Ge(IV)	322 ± 14	329 ± 33	261 ± 87
	Cs(I)	259 ± 44	281 ± 27	257 ± 70

Fig. 1. Scheme of SEArcularMINE process outline for saltworks bittern. Adapted from Filingeri et al. (2023).

2.5. Sorption/desorption columns set-up

After evaluating the kinetics in batch tests, column mode experiments were performed with transparent polyvinyl chloride (PVC) columns (100 mm length, 13 mm inner diameter, 67 mm max bed length) completely filled with the *N*-methylglucamine sorbents (2.8 ± 0.2 g). The inlet liquid was pumped upwards through the column with a peristaltic pump (Gilson Minipuls 3). At the exit of the column, a fraction collector (Gilson Fraction Collector FC 204) was installed to collect samples during the experiments.

To compare the results among all experiments, the data is presented as a function of the Pore Volume (PV), i.e. an equivalence that represents the void volume in the system. Therefore, the graphs are plotted as a function of the volume treated by the column along time converted as PV. It was determined by monitoring the conductivity at the outlet of the columns after pumping 10 mM NaCl at 0.5 mL/min through them, which after providing a breakthrough curve (see Fig. S2), allowed to determine that 1 PV was equivalent to 7.46 ± 0.85 mL by using the Eq. (2) (Simonnot et al., 2000).

$$1PV = Q \cdot t_b \tag{2}$$

where Q is the flow rate (mL/min) and t_b is the time to reach half of the maximum conductivity achieved in this test.

The experiments under column operation consisted of two steps: sorption and desorption. In the sorption stage, the bitterns were pumped through the column at 0.2 mL/min (1.62 ± 0.18 PV/h) (Figueira et al., 2022) until the sorbents got saturated and samples of 9 mL were periodically collected every 45 min. Then, desorption was performed by pumping 1 M HCl through the column at 0.05 mL/min (0.40 ± 0.04 PV/h) (Figueira et al., 2022) and samples of 5 mL were periodically collected each 100 min. After desorption with HCl, the columns were washed with deionised water. The sorbent was then regenerated by pumping 1 M NaOH through the columns. A final wash with deionised water was also performed to prepare the columns for the next experiment. To obtain the breakthrough and elution curves, the samples of the eluate of the column periodically collected were analysed by ICP-OES and ICP-MS. Breakthrough curves were obtained representing the relative concentration (C/C_0, where C_0 is the concentration of the synthetic bittern) against PV, while elution ones were constructed by representing the eluate concentration against PV. When the sorption stage was performed, the pH of the eluate of the column was also monitored.

Three main parameters were calculated from this type of experiments: (i) the sorption capacity (q_s) in $mg/g_{sorbent}$ or $\mu g/g_{sorbent}$, depending on the measured element concentration, to evaluate how much the sorbent can uptake each element in solution; (ii) the Concentration Factor (CF) for each element as a dimensionless parameter to quantify how much the eluate was concentrated with respect to the feed solution; and (iii) the Recovery ratio (R) in % to assess if during the elution stage it was able to completely recover all the elements sorbed in the sorbent. These three parameters are defined by the Eqs. (3), (4) and (5), respectively (Figueira et al., 2022; Reig et al., 2019).

$$q_s = \frac{m_s}{m_{sor}} = \frac{C_0 \int_0^{V_b} \left(1 - \frac{C}{C_0}\right) dV}{m_{sor}} \tag{3}$$

$$CF = \frac{\frac{1}{V_d} m_d}{C_0} = \frac{\frac{1}{V_d} \int_0^{V_d} C dV}{C_0} \tag{4}$$

$$R = 100\% \cdot \frac{m_d}{m_s} = 100\% \cdot \frac{\int_0^{V_d} C dV}{C_0 \int_0^{V_b} \left(1 - \frac{C}{C_0}\right) dV} \tag{5}$$

where m_s and m_d are the sorbed and desorbed mass (mg or µg) of the target element; C and C_0 are the target element measured concentration (mg/L or µg/L) at the outlet of the column and in the initial solution, respectively; V_b and V_d are the volume (L) of bittern and desorption

solution used in sorption and desorption stages; and m_{sor} is the mass (g) of sorbent used.

2.6. Mathematical modelling of ion exchange

The IX process dynamics were described with a mass transfer model based on: (i) the linear driving force model accounting for the intra-particle mass transfer resistance and (ii) a mass action law describing the equilibrium in the solid/liquid interface (Mazur et al., 2017). In order to describe the equilibrium between the solid and liquid phase concentrations, the sorption mechanism depending on the functional group was considered, and an equilibrium constant was defined accordingly. In a previous work (Vallès et al., 2023a), a speciation analysis was performed to determine the chemical species in which the target elements are present in the bittern at the working pH and the sorption mechanism was postulated for each one. The following sections present the model assumptions and governing equations for batch and packed bed columns.

2.6.1. Dynamic modelling of ion exchange kinetics in a batch system

The mass transfer model for IX kinetics on a batch system was developed assuming an isothermal system where the mass transfer resistance in the hydrodynamic film surrounding the particles is neglected, and the particles are considered as unidimensional thin plates. The IX kinetics on a batch system is described by the mass conservation balance inside the solid phase, which is given for the linear driving force model as (Mazur et al., 2017):

$$\frac{dq_j}{dt} = k_{p,j} a_p \left(q_j^* - q_j\right) \tag{6}$$

where $k_{p,j}$ is the mass transfer coefficient for intraparticle diffusion of species j (cm/s), a_p is the specific area of the thin plate particles (1/cm), q_j is the average concentration of species j in the solid phase at a time t (mEq/g) and q_j^* is the solid phase concentration of species j in equilibrium with C_j (mEq/g), given by the mass action law.

Moreover, the mass conservation balance to the batch system is given by (Mazur et al., 2017):

$$V\frac{dC_j}{dt} + W\frac{dq_j}{dt} = 0 \tag{7}$$

where C_j is the concentration of species j in the liquid phase at a time t (mEq/L), q_j is the average concentration of the species j in the solid phase at a time t (mEq/g), V is the volume of the solution (L), and W is the sorbent dry weight (g).

The initial conditions for both equations are (Mazur et al., 2017):

$$C_j = C_{j,0} \tag{8}$$

$$q_j = q_{j,0} \tag{9}$$

2.6.2. Dynamic modelling of ion exchange kinetics in a packed bed column

The modelling of IX in a packed bed column requires considering diffusion and convection, besides the intraparticle mass transfer described in the previous section. In addition, the pressure variations along the packed bed column are neglected, and the liquid phase is axially dispersed by a plug flow. Given these assumptions, the mass transfer conservation in the fluid around the particles is described by (Mazur et al., 2017):

$$\frac{\partial C_j}{\partial t} = D_{ax}\frac{\partial^2 C_j}{\partial z^2} - u\frac{\partial C_j}{\partial z} - \frac{(1-\varepsilon)}{\varepsilon}\rho_p f\frac{dq_j}{dt} \tag{10}$$

where C_j (mg/L of fluid) is the concentration of species j in the liquid phase, t (s) is the time, D_{ax} (cm^2/s) is the axial dispersion coefficient, z (cm) is the axial bed position, u (cm/s) is the interstitial fluid velocity, ε is the bed porosity (−), ρ_p is the particle density (g/L on a dry basis), f is the swelling factor (volume of the dry particle divided by the volume of the wet particle) and q_j (mg/g of sorbent) is the concentration of species j in the solid phase. The mass conservation inside the particles (linear drive force model) is described by Eq. (6), as seen in the previous section.

Finally, the initial and boundary conditions used for the sorption process are described in Eqs. (11)–(14) (Mazur et al., 2017).

$$At\ t = 0, C_j = 0 \tag{11}$$

$$At\ t = 0, q_j = 0 \tag{12}$$

$$At\ z = 0, uC_{0,j} = uC_j - D_{ax}\frac{\partial C_j}{\partial z} \tag{13}$$

$$At\ z = L, \frac{\partial C_j}{\partial z} = 0 \tag{14}$$

where $C_{0,j}$ (mg/L of fluid) is the feed concentration of species j, and L is the bed height (m).

These equations can also describe the desorption process, but with appropriate initial and boundary conditions described by Eqs. (15) and (16) (Mazur et al., 2017):

$$At\ t = 0, C_j = C_{j,D0} \tag{15}$$

$$At\ t = 0, q_j = q_{j,D0} \tag{16}$$

where $C_{j,D0}$ is the initial concentration of species j in the liquid phase at the beginning of the desorption stage and $q_{j,DO}$ is the initial concentration of species j in the solid phase at the beginning of the desorption stage.

2.7. Analytical techniques

Electrical conductivity (EC) and pH were monitored using a glass electrode EC-meter (GLP 31, CRISON) and pH-meter (GLP 22, CRISON), respectively. The elemental composition of the samples was analysed by ICP-OES (5100 IPC-OES, Agilent Technologies) and ICP-MS (7800 ICP-MS, Agilent Technologies). Samples were diluted with 2 % HNO_3 and filtered through 0.22 μm before analysis.

In addition, the concentration of Cl^- and Br^- in the samples was determined by ion chromatography. Dionex ICS-1100 with the anion exchange IONPAC® AS23 column was used with a mobile phase of 4.5 mmol/L Na_2CO_3 and 0.8 mmol/L $NaHCO_3$ as an eluent solution.

3. Results and discussion

3.1. Characterisation of the sorbents by the kinetic performance

Fig. S3 (Supplementary Information) shows the experimental results obtained in the kinetic tests by plotting the sorption (Eq. (1)) as a function of the experimental time for the CRB03 (Fig. S3.a), CRB05 (Fig. S3.b) and S108 (Fig. S3.c) using the bittern 1, the one expected at the TEs-unit containing Ca and Mg. In order to simplify the graphs, only those elements that have been extracted (i.e. Co, Ga, Ge and B) were plotted. All the others were not sorbed by the sorbent (sorption ≤5 %).

For the CRB03 sorbent (Fig. S3.a), it can be observed that within the first 20 min of the test, the 98 % Ge and 93 % B were already extracted, with low co-extraction of Co (43 %) and Ga (19 %). As time passed, the sorption slowly increased for the different elements in the solution, especially for Co and Ga. For instance, the extraction at equilibrium (after 24 h) slightly increased for B (99.3 %) and Ge (99 %), whereas it was possible to achieve sorption values of 87 % for Co and 30 % for Ga. Due to the IX process, the pH of the solution tended to increase from 6.98 up to 8.67 at the end of the test, which can be related to the release of hydroxyl groups from the structure of the sorbent when sorbing species such as H_3BO_3 or H_4GeO_4 (Vallès et al., 2023a), which can interact with

the free Na^+ ions and slightly basify the solution.

Concerning the CRB05 (Fig. S3.b) a similar trend was observed, but exhibiting a worse performance compared to the CRB03. It can be observed that the sorption for the elements mentioned above after 20 min of test was lower than the CRB03. For example, the extraction of Ge and B were 85 % and 76 %, respectively, with lower co-extractions of Co (35 %) and Ga (14 %). However, after 24 h, similar sorption was achieved: B (99 %), Ge (98.9 %), Co (75 %) and Ga (33 %). The same trend was observed regarding the pH, increasing from 7.04 to 8.76 at the end of the test.

Finally, the extraction of B, Ge, Co and Ga was also achieved using the S108 (Fig. S3.c). However, in this case, the S108 showed the worst performance in sorption, with extraction values of 70 % for Ge, 62 % for B, 25 % for Co and 7 % for Ga after 20 min of experiment. The sorption tended to increase slowly as time passed, reaching 99.7 %, 99 %, 55 % and 23 % of extraction for Ge, B, Co and Ga after 24 h of experiment. In this case, also, the pH tended to increase, reaching a value of 8.35 at the end of the test (initial pH 6.98).

As has been aforementioned, within the first 20 min of the kinetic tests, the B extraction was around 93 % for CRB03, 76 % for CRB05 and 62 % for S108. In comparison to the literature, it was noticed that those values were higher than the ones obtained by Figueira et al. (2022) (around 37 % sorption in the first 20 min). Although the B concentration from their feed solution (50 mg/L) was lower than the one from the bittern 1 used in these kinetic tests (121 mg/L), it is expected that the main reason for this difference is related to the solid/liquid ratio used (30 $g_{sorbent}$/L in the present study in front of 3 $g_{sorbent}$/L in the tests performed by Figueira et al.). Similarly, Nishihama et al. (2013) conducted a kinetic experiment with conditioned CRB03 and CRB05 with a solid/liquid ratio of 2 $g_{sorbent}$/L and B concentration around 54 mg/L. They reported the need of around 5 h for CRB03 and 6.5 h for CRB05 to achieve 90 % of equilibrium sorption. Ipek et al. (2009) successfully applied the sorbent CRB02 with the same solid/liquid ratio (2 $g_{sorbent}$/L) to remove B from geothermal water with 8.5–13 mg B/L. In their kinetic tests, only 2 h were needed to attain a sorption of 90 %, which was also the necessary time for S108 in the current study. However, similar results were obtained by Darwish et al. (2015), where only 10 min were required to attain the 90 % sorption when evaluating the Amberlite IRA743 sorbent (2 $g_{sorbent}$/L) in front of a pure B solution (5 mg/L). Cyganowski et al. (2021) compared the kinetic performance of a synthesised sorbent with *N*-methylglucamine (2PTN) and CRB05 when targeting B removal from a geothermal water containing 11 mg/L of B. They reported that, despite 2PTN (16 $g_{sorbent}$/L) being able to remove 91 % of B in 60 min, CRB05 (4 $g_{sorbent}$/L) only needed 10 min to remove the 94 % of B.

3.2. Assessment of the sorbents' performance under column operation

3.2.1. Determination of the breakthrough and elution profiles

Fig. 2 shows the profiles of the breakthrough and elution curves as a function of the volume treated expressed as PV when treating the bittern 1 (i.e. the brine containing Ca and Mg) for the three *N*-methylglucamine sorbents. The data related to the major elements in the solution (e.g. Na, K, Mg, Ca and S(VI)) could be found in the Supplementary Information (Fig. S4), as most of these elements presented low affinity for the sorbents considering their concentration in the bittern and their performance compared with the TEs. Additionally, those elements extracted by the sorbent (i.e. B, Co, Ga and Ge) were fitted by a mass transfer model, represented with a continuous line.

In relation to the breakthrough curves, it was observed that Li, Rb, Sr and Cs were not retained in the sorbent ($C/C_0 = 1$). Therefore, the ones observed were in the following order according to the breakthrough point: Co, B, Ge and Ga, except for the CRB05, where Ga was the first element to be saturated on the sorbent. For example, regarding Co, its breakthrough was observed at 2 PV for the S108 and CRB03, while in the CRB05, it took place at 12 PV. Then, concerning B, the breakthrough took place at around 12 PV for the three sorbents, being saturated at 20 PV (62 PV for the CRB05). This highlighted a higher sorbent capacity of the CRB05 towards B than the other sorbents tested. In the case of Ga, the breakthrough was observed at the first PV treated with the CRB05, while it was continuously sorbed into the S108 and CRB03; no breakthrough was observed within the 75 PV treated. Finally, for the Ge, the breakthrough for the three sorbents was observed at around 15 PV, but the sorbent was not completely saturated on it after 75 PV (C/C_0 around

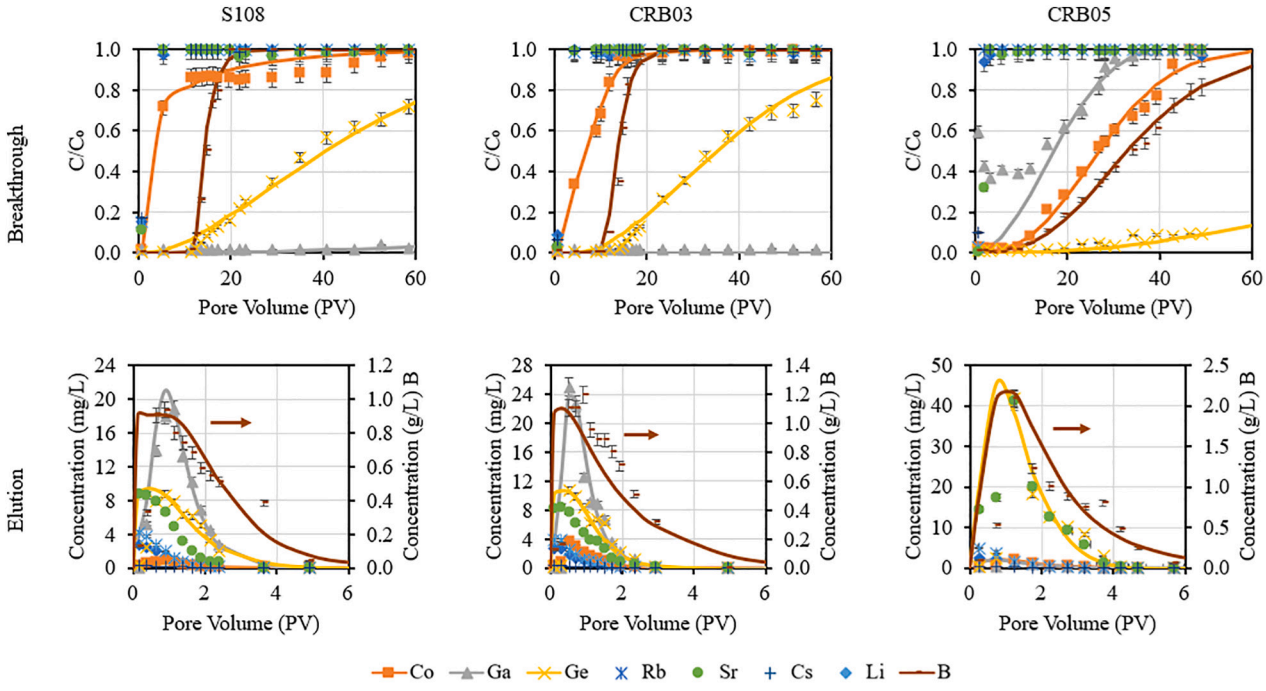

Fig. 2. Breakthrough and elution curves of TEs as a function of the pore volume for the S108, CRB03 and CRB05 sorbents using the bittern 1. Sorption: 1.62 ± 0.18 PV/h. Elution: 0.40 ± 0.04 PV/h using 1 M HCl.

0.8 for S108 and CRB03, and 0.2 for CRB05).

Regarding the elution curves, it was observed that starting at 0.1 PV, Co was eluted entirely using 1 M HCl within the first 3 PV, and Ga and Ge were also fast desorbed (3.5 PV). However, B required up to 5 PV (6 PV for CRB05) to be completely removed from the sorbent. The B concentration in the eluate reached values around 0.9 g/L, 1.2 g/L and 2.1 g/L for the S108, CRB03 and CRB05, respectively. Regarding the other TEs, it should be noted that their concentration increased to mg/L levels (compared to around 275 μg/L initially in the bittern). Additionally, the maximum concentration of Ga reached was around 19 mg/L and 25 mg/L for the S108 and CRB03, respectively, while in the CRB05 was 1.6 mg/L. The opposite trend was observed for Ge, with concentrations of 42 mg/L in the case of CRB05 and lower values for the S108 (8.7 mg/L) and CRB03 (10.7 mg/L). However, the maximum concentration of Co reached was below 3.6 mg/L.

The results for bittern 2, the one without Ca and Mg expected at the TEs-unit, are collected in Fig. 3. As in the previous case, the major elements can be found in the Supplementary Information (Fig. S5).

In relation to the breakthrough curves, the three sorbents followed the same order: Ga, Co, B and Ge. In the three cases, the breakthrough curve for Ga was observed around 10–19 PV, with the sorbent completely saturated at 25–36 PV. The breakthrough of Co took place at 20–24 PV (30 PV for CRB05), and the sorbent was completely saturated on it after 34 PV (30 PV in the case of CRB03). The breakthrough for B was displaced to 25 PV for the S108 and CRB03, while it was allocated at 30 PV for the CRB05. In this case, the sorbent was completely saturated on B at 34 PV for the S108 and CRB03, while for the CRB05, that point was observed at 46 PV. Finally, the breakthrough for Ge started at 30 PV for the three sorbents, but they never got saturated on it after treating up to 100 PV.

Similar to the previous case, the elution of the sorbents was completely achieved within 4 PV of HCl (6 PV for S108). In this case, two double peaks were observed in the CRB03 for B and Ge, which suggested that the efficiency of the sorbent could have been affected by the channelling effect (i.e. the solution would preferentially flow along specific paths through the sorbent bed inside the columns, which would result in the solution not contacting the total amount of sorbent available) (Mestri et al., 2023) or due to a two different bonds between the sorbent and the sorbed species, such a chelate ring or hydrogen bonds (Wen et al., 2016). Looking at the highest concentration peaks attained in the elution, all were in the order of g/L, such as 2.8 g/L for CRB05, followed by the CRB03 (1.9 g/L) and S108 (1.8 g/L). After B, the Ge presented the highest concentration, reaching 37 mg/L for CRB05 and 17 mg/L for both S108 and CRB03. In this case, the Ga concentrations were relatively lower, being below 1 mg/L for CRB03 and CRB05, while for S108 it reached a maximum value of 2.4 mg/L. Finally, with this sorbent, it was possible to achieve the highest concentrations of Co, ranging between 2.7 and 3.6 mg/L.

Finally, Fig. 4 shows the breakthrough and elution curves for the sorbents when treating the bittern 3, which simulates that B would be extracted without any pre-treatment stages. Major elements are included in the Supplementary Information (Fig. S6).

Generally, the saturation curves followed the same trend, being first saturated on Co, then on Ga (except for the CRB05), later on B and finally on Ge, which never gets to saturate the sorbent completely. In relation to their behaviour, it was observed that the saturation on Co happened at low PV (<15 PV). Then, the breakthrough point for B was also displaced to lower values due to its higher concentration in the bittern: at 6 PV, 5.9 PV and 3.1 PV for S108, CRB03 and CRB05, respectively, while its complete saturation was at 34 PV, 31.6 PV and 61.7 PV for the sorbents in the same order previously mentioned. Concerning the other two minor elements, Ga followed a similar trend to B, but in the case of Ge the breakthrough took place at 10 PV, but the sorbent was not saturated on it even after treating 100 PV of bittern.

About elution, it was observed that the sorbents were completely regenerated after 8 PV, 4 PV and 6 PV of 1 M HCl for S108, CRB03 and CRB05, respectively. Looking at the concentration, the B in the eluate reached 1.5 g/L, 2.2 g/L and 1.7 g/L for the S108, CRB03 and CRB05. A double peak was also observed in the case of the elution of S108. The other TEs (i.e. Co, Ga and Ge) were also noticeably concentrated in the solution, reaching concentrations in the order of mg/L. Ge was the element that reached the highest concentration (6.8 mg/L, 9.3 mg/L and

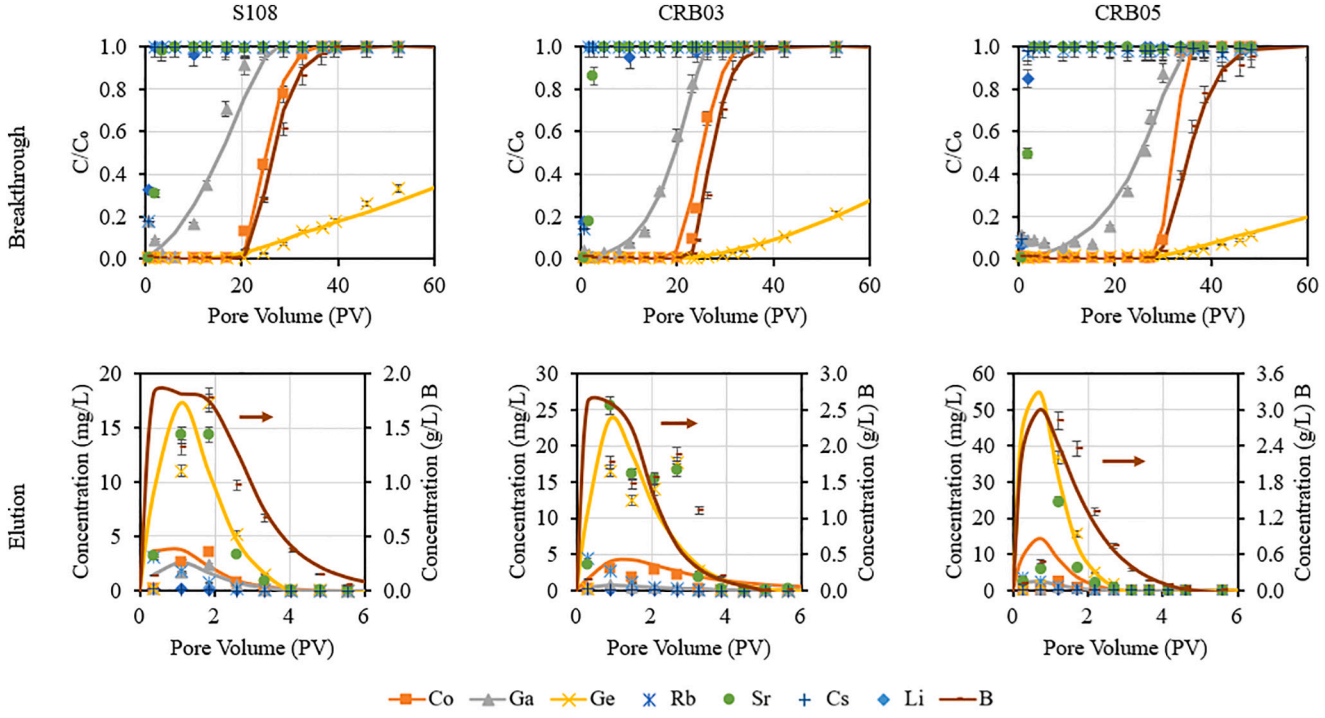

Fig. 3. Breakthrough and elution curves of TEs as a function of the pore volume for the S108, CRB03 and CRB05 sorbents using the bittern 2. Sorption: 1.62 ± 0.18 PV/h. Elution: 0.40 ± 0.04 PV/h using 1 M HCl.

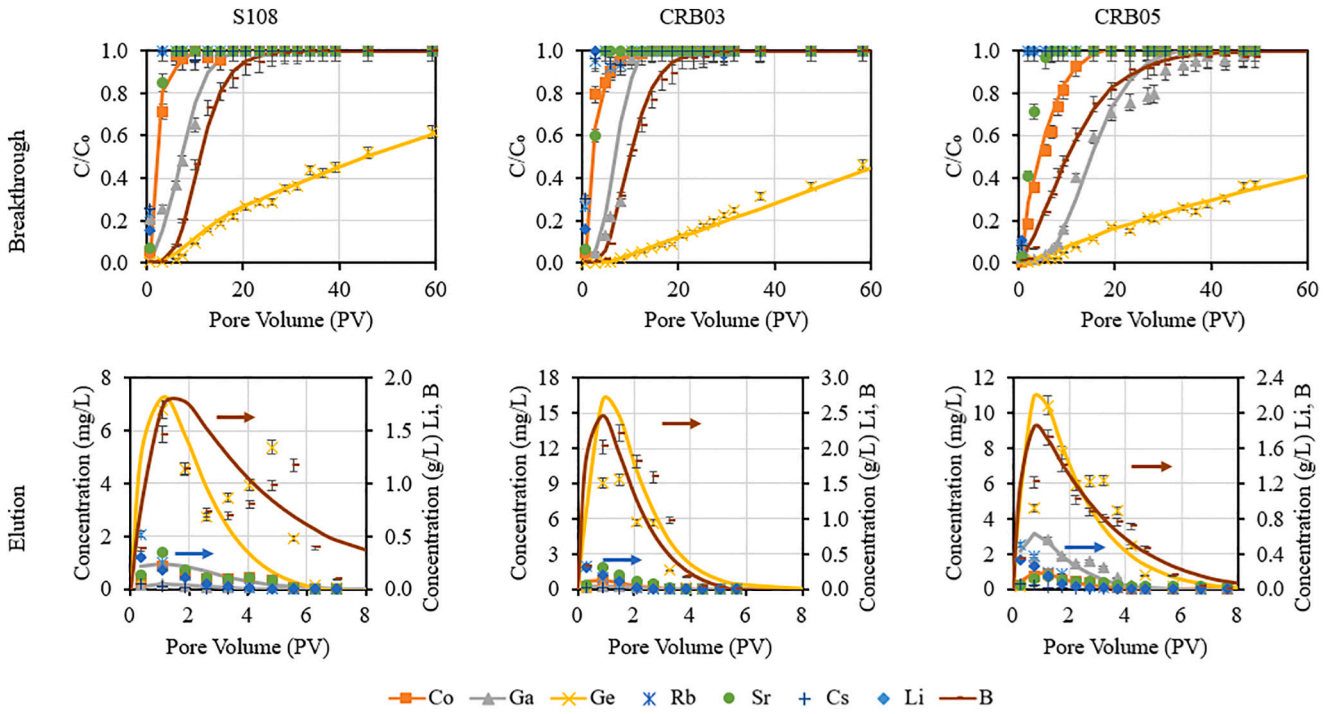

Fig. 4. Breakthrough and elution curves of TEs as a function of the pore volume for the S108, CRB03 and CRB05 sorbents using the bittern 3. Sorption: 1.62 ± 0.18 PV/h. Elution: 0.40 ± 0.04 PV/h using 1 M HCl.

10.4 mg/L for the S108, CRB03 and CRB05, respectively). Following Ge, a noticeable peak of Ga was observed in the elution of the CRB05 (around 2.8 mg/L), while the concentration of the CRB03 and S108 remained below 0.22 mg/L. Due to the fast breakthrough for Co, its concentration remained below 1 mg/L in the three eluates obtained.

3.2.2. Comparison of the performance of the sorbents: sorbent capacity, concentration factor and recovery ratio

As a general observation, all sorbents got first saturated on Ga. Then, the breakthrough of Co was attained, followed closed by B. And, Ge was the last element in saturating the sorbents. However, some exceptions can be observed. For example, when evaluating bittern 3, the three sorbents were first saturated on Co instead of Ga. This fact could be explained according to the elevated content on Mg, as it is worth noticing that Mg content for that bittern was at the g/L level. Despite the low affinity that the sorbents presented towards it during their performances, the high Mg content caused the ionic strength of bittern 3 to increase to almost double ($I = 7.3$) that of bittern 1 ($I = 3.8$) or 2 ($I = 4.3$). It was previously reported by Louati et al. (2016) that a variation in the ionic strength can modify the selectivity of the ion exchangers. Additionally, Simonnot et al. (2000) provided a large range study in which it was demonstrated that the volume of liquid that could be treated by a column filled with a *N*-methylglucamine sorbent strongly depended on the concentration of B in the feed solution. Therefore, as B concentration increased, the breakthrough was displaced to the left, which was also observed for bittern 3 (363 mg/L of B) compared to bitterns 1 and 2 (121 mg/L of B). They reported that around 14 BV (equivalent to the PV parameter reported in this study) could be treated for a single B feed solution of 100 mg/L using the sorbent Amberlite IRA743. That was approximately also observed in the current research for the bittern 1. Moreover, according to the pH profile observed in the sorption stage (see Fig. S7.a in Supplementary Information), S108 and CRB03 sorbents were in a slightly acidic form when evaluating bittern 1. This fact strongly affected the performance of Co, whose breakthrough curve was also displaced to the first element that was sorbed, and Ga, which was being continuously sorbed by both sorbents.

Once the three bitterns have been evaluated while testing the three sorbents, the performance parameters (sorbent capacity, concentration factor and recovery ratio) were determined to compare the performance under different scenarios.

The sorption capacity for each sorbent and solution was calculated according to Eq. (3) and reported in Table 1. Consequently, several evidences have been observed. First, the low sorption capacity for B in the first test performed with S108 and CRB03 (the one evaluating bittern 1) can be explained, as already mentioned above, according to the pH profile observed in the sorption stage (see Fig. S7.a), which suggests that these two sorbents were in a slight acidic form in that test. In addition, after having the sorbent regenerated for the first time, B sorption capacity is not strongly affected by the matrix composition of the feed solution. Thus, an average value of 8.3 mg/g was obtained for S108 and around 11 mg/g for both CRB03 and CRB05. These capacities were higher than the one obtained by Ipek et al. (2009) when they evaluated CRB02 with geothermal water containing 12–13 mg B/L, for which they obtained a total sorption capacity of around 5 mg/g. The obtained capacities in this study were also in the expected range, as Figueira et al. (2022) reported Langmuir maximum sorption capacities of 11, 15 and 12 mg/g for S108, CRB03 and CRB05, respectively, and around 13 mg/g for CRB03 after testing it in column mode. Second, Co and Ge sorption decreased when potential competitors, such as Ca and, especially, Mg, were found in the feed solution. Finally, and as mentioned earlier, the slight acidic form that S108 and CRB03 seemed to present when evaluating the bittern 1 could explain the difference in Ga retention for both sorbents. Thus, considering the results obtained with the bittern 2 (with less ion competence and with the sorbent in the non-acidic form), the sorption capacity of the TEs that were sorbed followed the order B >> Ge > Co > Ga. However, whereas CRB03 and CRB05 presented similar results, S108 presented lower sorption capacities.

The values of concentration factors (CFs) are represented in Fig. 5.a, grouped on the sorbent used and the bittern treated. The highest CFs achieved were attained for Ge, ranging from 13 for the S108 sorbent, treating the bittern with Ca and Mg (bittern 1), to 35 for the CRB03, for the bittern without Ca and Mg (bittern 2). Looking at B, the highest CFs

Table 1
Sorption capacities for minor elements or TEs. The table did not include major elements, as they had no affinity with the sorbent.

Sorbent	Bittern	Sorption capacity (μg/g)							Sorption capacity (mg/g)		
		Li	Co	Ga	Ge	Rb	Sr	Cs	B	Ca	Mg
S108	1	0.4	6.5	41	33	0.0	0.0	0.0	3.8	0.5	0.4
	2	0.0	17	9.2	56	0.0	4.1	0.0	7.6	0.1	0.0
	3	0.0	1.2	3.0	27	0.0	0.2	0.0	9.0	0.4	2.5
CRB03	1	2.5	7.7	48	42	1.2	0.4	0.0	5.2	0.2	0.0
	2	0.0	23	17	78	0.0	7.7	0.0	12	0.1	0.1
	3	0.0	1.6	4.8	45	0.4	0.7	0.0	13	0.7	11
CRB05	1	0.7	21	12	116	0.0	19	0.0	9.1	0.2	0.5
	2	0.1	27	13	92	0.2	2.5	0.0	11	0.0	0.1
	3	0.0	3.0	13	67	0.0	0.5	0.0	12	0.6	7.9

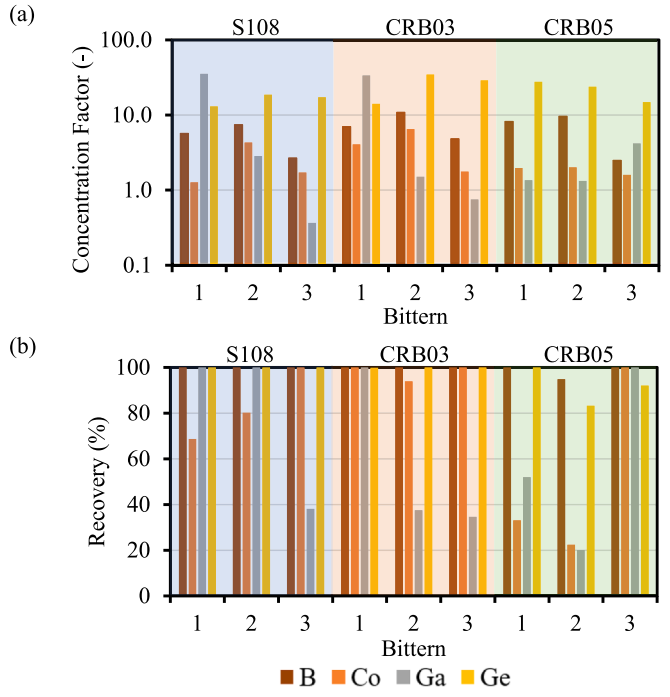

Fig. 5. Comparison of the (a) concentration factors and (b) recovery achieved depending on the bittern treated and the *N*-methylglucamine sorbent used.

were normally achieved for the CRB03, ranging from 4.8 for the bittern without pre-treatment (bittern 3) to 11 with the bittern 2. With the exception of an 8.2 achieved for bittern 1, CRB05 exhibited slightly lower CFs, while the ones achieved for the S108 were the lowest ones. About Ga, it was possible to concentrate it by a factor of 35 and 34 for the bittern 1 with the S108 and CRB03, respectively. In the other cases, the CFs ranged between 0.3 and 4.2. Finally, in most of the cases, the CFs for Co moved between 1.3 and 2.0, and it was possible to achieve higher values in bittern 2 for CRB03 (6.5) and S108 (4.3) and in bittern 1 for the CRB03 (4.1).

In addition to sorption capacity and CF, the recovery of the elements after applying the desorption stage was also calculated and represented as a percentage in Fig. 5.b. In almost all the cases, the elements that were sorbed (i.e. B. Co, Ga and Ge) were recovered entirely (>90 %). Those values, at least for B for which the *N*-methylglucamine sorbents are normally targeted, were in the expected range, as Jung and Kim (2016) reported a B desorption efficiency of 87 % using 0.25 M HCl. The non-ful recovery of the elements from the sorbent may be related to a strong interaction between the component and the sorbent. However, it must be noticed that after the acid desorption step, 1 M NaOH was pumped through the column, followed by several washes with deionised water. Thus, as suggested by their suppliers, the sorbents would be suitably conditioned for the next experiment.

As *N*-methylglucamine sorbents have been generally applied for B removal/recovery, a comparison of column performances in different studies, including some of the ones presented in this manuscript, is shown in Table 2 (Nishihama et al., 2013; Figueira et al., 2022; Bonin et al., 2021; Shao et al., 2023; Altıok et al., 2023). Several parameters have been reported in the table, such as the sorption capacity, the PV needed to saturate the sorbent, the maximum concentration achieved in elution and the amount of B recovered from the sorbent.

3.2.3. Sorption and desorption modelling performance

Table 3 shows the estimated model parameters for the batch kinetic experiments in terms of selectivity coefficients (*K*) and the mass transfer coefficients for intraparticle diffusion ($k_p \cdot a_p$) for the evaluated sorbents. The modelling results (see lines in Fig. S3) generally showed a strong agreement for B and Ge ($r^2 > 0.97$), whereas some deviations were obtained for Co and Ga. For instance, the model predicted that Co sorption for the sorbents CRB03 and CRB05 would be faster, attaining the equilibrium in 1 h, which produces significant discrepancies ($r^2 = 0.68$ and $r^2 = 0.78$, respectively). Conversely, the model described a slower Co sorption in the case of S108, so only the process after 3 h was accurately reproduced. In the case of Ga, the model also presented a slower IX and more significant discrepancies, leading to lower squared correlations for CRB03 and CRB05 ($r^2 = 0.37$ and $r^2 = 0.55$, respectively). Despite these deviations, the selectivity coefficients estimated followed the expected order according to the experimental trends. Therefore, the values obtained for B and Ge were the highest and similar to each other, followed by Co and, finally, Ga, which exhibited the least affinity. Regarding the mass transfer coefficient, it can also be observed that the lowest value was obtained for Co, which was the one that took the longest time to reach the equilibrium. For the other elements, the order was Ga, Ge and B. However, the values were close to each other, which aligned with the experimental data that presented no significant differences for those elements. The complex nature of the *N*-methylglucamine groups should be stressed, involving different atoms with different properties. Additionally, the expected species of Co, Ga and Ge in solution, as complex structures with hydroxyl and chloride ions, and bulky species typically associated with IX reactions were not as fast as when strong IX sorbents are involved.

Concerning the dynamic modelling of IX in a packed bed column, Table 4 presents the estimated parameters in the different scenarios. The model described the breakthrough curves well for all the elements within the scenarios evaluated, as shown in Figs. 2–4 (see lines), where the R-squared values were above 0.97 in all the cases. However, the model exhibited some deviations in the elution processes, especially noticeable for B and Ge. In particular, the double peaks observed for these elements in the CRB03 cannot be fitted by the model because the model's physics formulation did not account for the reasons that generated the double peaks, probably caused by two different sorption mechanisms, as previously discussed. The selectivity coefficients reflected the affinity of each element with the sorbent depending on the scenario. For instance, the order obtained for bittern 1 and sorbents

Table 2
Comparison of several column performances that applied *N*-methylglucamine sorbents targeting B removal/recovery.

Sorbent	Solution composition	Experimental conditions	PV needed for saturation	Peak achieved in elution	Sorbent capacity	Recovery (R) Concentration factor (CF)	Reference
CRB05	B: 800 mg/L	Sorption: 9.4 PV/h	18 PV	–	12.8 mg/g LMS	–	(Nishihama et al., 2013)
Chelest Fiber	B: 800 mg/L	Sorption: 8.6 PV/h Elution: 2 M HCl	17 PV	4.5 g/L 2.3–6.3 PV	12.4 mg/g LMS	R: 99.5 %	(Nishihama et al., 2013)
Chelest Fiber	B: 850 mg/L Li: 1.4 g/L Mg/K: ≈20 g/L Na: 61 g/L	Sorption: 8.3 PV/h Elution: 2 M HCl	21 PV	5.4 g/L	12.4 mg/g LMS	R: 81.7 %	(Nishihama et al., 2013)
CRB03	B: 50 mg/L	Sorption: 1.8 PV/h Elution: 1 M HCl, 0.45 PV/h	130 PV	2.9 g/L	12.9 mg/g	R: 98 % CF: 30	(Figueira et al., 2022)
Amberlite IRA743	1600 mg_B/L Li/Ca: ≈1 g/L Mg: 3.1 g/L K/SO_4^{2-}: ≈13 g/L Na: 103 g/L Cl: 183 g/L	Sorption: 0.1, 0.5, 1 and 3 PV/h	3.5 PV at 0.1 PV/h	–	6.53 mg/g	–	(Bonin et al., 2021)
D403	B: 490.8 mg/L Li/Na/K/Ca/Mg: 1 g/L	Sorption: 150 min, 10 mL/min Elution: 5 mL/min 1 PV = 60 mL	25 PV	3.7 g/L	8.23 mg/g	R: 98.2 %	(Shao et al., 2023)
CRB05	B: 10.94 mg/L HCO_3^-: 0.7 g/L Na/Cl/SO_4^{2-}: ≈0.2 g/L	Sorption: 20 PV/h Elution: 0.526 M H_2SO_4, 10 PV/h	900 PV	0.6 g/L 4–20 PV	8.39 mg/g	R: 90.4 %	(Altıok et al., 2023)
S108	B: 121 mg/L Bittern 2	Sorption: 1.6 PV/h Elution: 1 M HCl, 0.4 PV/h	34 PV	1.8 g/L 1–6 PV	7.6 mg/g	R: >99 % CF: 7.4	This study
CRB03	B: 121 mg/L Bittern 2	Sorption: 1.6 PV/h Elution: 1 M HCl, 0.4 PV/h	34 PV	1.9 g/L 1–4 PV	11.5 mg/g	R: >99 % CF: 10.9	This study
CRB05	B: 121 mg/L Bittern 2	Sorption: 1.6 PV/h Elution: 1 M HCl, 0.4 PV/h	46 PV	2.8 g/L 1–4 PV	11.1 mg/g	R: 95 % CF: 9.6	This study

LMS: Langmuir Maximum Sorption capacity.

S108 and CRB03, $K_{Co} < K_B < K_{Ge} < K_{Ga}$, agreed with the selectivity observed experimentally. These sorbents did not reach saturation in Ga, whereas in the case of CRB05 it was the first element to be completely sorbed. As explained above, the measured pH profile indicated that S108 and CRB03 were slightly acidic when evaluating bittern 1, affecting Co and Ga performance. In an acidic media, the protonation of functional groups on the *N*-methylglucamine sorbents (hydroxyl groups) occurred, diminishing the binding of Co^{2+}. Conversely, the increased protonation led to a stronger electrostatic interaction with the negatively charged Ga $(OH)_4^-$ complex, consequently increasing Ga sorption. The model captured the differences observed experimentally on Ga sorption since, as seen in Table 4, the selectivity coefficients for Ga were the highest for S108 and CRB03 and the lowest for CRB05 in the case of bittern 1. Likewise, the mass transfer coefficient for intraparticle diffusion generally correlated with the observed patterns. The mass transfer coefficient for intraparticle diffusion is a parameter that quantifies the rate at which a solute undergoes diffusion within the interstices of the sorbent material. Therefore, the shape of the breakthrough curves is related to the mass transfer coefficients: a lower mass transfer coefficient indicates a slower solute diffusion within the sorbent, so it takes longer to

Table 3
Estimated values for mass transfer coefficient and the specific area of the thin plate particles ($k_p \cdot a_p$) and selectivity coefficient (K) during the mathematical modelling of kinetics in a batch system.

TE	$k_p \cdot a_p \cdot 10^{-2}$ $\left({}^{1}/_{min}\right)$			$K\,(-)$		
	CRB03	CRB05	S108	CRB03	CRB05	S108
Co	1.51	1.54	1.51	2.028	2.076	0.903
Ga	6.03	6.05	6.33	0.173	0.222	0.190
Ge	7.21	7.52	7.25	40.179	30.144	30.529
B	8.45	8.43	4.52	40.023	30.017	25.007

Table 4
Estimated values for mass transfer coefficient and the specific area of the thin plate particles ($k_p \cdot a_p$) and selectivity coefficient (K) during the mathematical modelling of kinetics in a packed bed column.

		$k_p \cdot a_p \cdot 10^{-2}$ $\left({}^{1}/_{min}\right)$			$K\,(-)$		
Sorbent	TE	Bittern 1	Bittern 2	Bittern 3	Bittern 1	Bittern 2	Bittern 3
S108	Co	0.19	5.38	0.61	0.004	0.024	0.001
	Ga	0.09	0.48	0.76	0.175	0.013	0.008
	Ge	0.35	0.20	0.13	0.029	0.086	0.078
	B	7.56	6.01	1.22	0.009	0.025	0.014
CRB03	Co	0.68	1.24	0.61	0.006	0.041	0.003
	Ga	0.11	0.39	0.93	0.349	0.026	0.013
	Ge	0.47	0.33	0.13	0.034	0.142	0.179
	B	9.03	15.01	0.83	0.012	0.045	0.023
CRB05	Co	0.39	6.93	0.64	0.030	0.045	0.006
	Ga	0.31	0.25	1.13	0.016	0.032	0.022
	Ge	0.11	0.19	0.08	0.172	0.170	0.144
	B	0.34	3.93	0.45	0.038	0.054	0.017

achieve saturation. As shown in Table 4, the minimum values for each sorbent and bittern tested were observed for Ge in most cases, consistent with the fact that Ge manifested the lengthiest breakthrough time. The only exception occurred in the cases of sorbents S108 and CRB03 tested with bittern 1 (see Fig. 2), where no breakpoint was observed for Ga. Consequently, the mass transfer values were the lowest in these instances. B breakthrough curve in those cases was sharper than for Co, Ga and Ge. Therefore, the mass transfer coefficients for B were higher than for the other TEs. However, Ga, Co and B presented similar breakthrough curves for sorbent CRB05 with bittern 1; thus, the values estimated for these TEs were also quite similar. Analogous reasoning applies to the remaining instances. As mentioned above about the fitting of kinetics in a batch system, it is important to note that the complexity of the system, dealing with multiple species, competitive binding and dynamic conditions, introduce challenges in accurately representing all interactions.

4. Conclusions

The current research assessed the performance of S108, CRB03 and CRB05 (commercial *N*-methylglucamine sorbents) in extracting various TEs from seawater saltworks bitterns. The three sorbents revealed a notable affinity not only for the previously established B but also for Co, Ga, and notably Ge. Both B and Ge exhibited the fastest sorption kinetics, reaching equilibrium (>90 %) in less than an hour, except for S108, which required 2 h. Column mode experiments revealed that 20–25 PV of bittern could be effectively treated to remove B and Ge from brine solutions before sorbents' saturation. However, the presence of competitors decreased the treatable volume, significantly displacing Co's breakthrough to the left, indicating a reduced affinity. Acidic elution using 1 M HCl achieved CFs up to 35 and 11 for Ge and B, respectively, with similar efficiency (35) observed for Ga when sorbents were in their acid form during sorption. This elution method facilitated >90 % recovery of almost all initially sorbed elements. The implemented model integrating equilibrium and kinetic sorption mechanisms between *N*-methylglucamine functional groups and TEs successfully replicated the experimental trends in batch and dynamic systems. The present study's findings underscore the efficacy of *N*-methylglucamine sorbents as an environmentally friendly approach for extracting CRMs from saltworks bitterns. Furthermore, it highlights the opportunity for valorising these brines, traditionally considered waste.

Considering the level of the research done at the laboratory, and despite the fact that a large effort has been devoted to evaluating different types of bittern compositions, it is mandatory to assess the sorbents' performance in pilot tests to identify possible weaknesses. These trials will assess the efficiency and workability over long periods (e.g. 6 to 12 months) using, in addition, real bitterns. The possible implications of other minor components on the properties of the sorbents, not evaluated in this laboratory research, will identify potential weaknesses of the approach.

CRediT authorship contribution statement

V. Vallès: Writing – original draft, Methodology, Investigation, Data curation. **M. Fernández de Labastida:** Writing – review & editing, Software, Methodology, Data curation. **J. López:** Writing – review & editing, Validation, Supervision, Conceptualization. **J.L. Cortina:** Writing – review & editing, Validation, Supervision, Resources, Project administration, Funding acquisition, Conceptualization.

Declaration of competing interest

The authors declare that they have no known competing financial interests or personal relationships that could have appeared to influence the work reported in this paper.

Data availability

The data will be available in Zenodo.

Acknowledgements

This work was supported by the EU within SEArcularMINE (Circular Processing of Seawater Brines from Saltworks for Recovery of Valuable Raw Materials) project – Horizon 2020 programme, Grant Agreement No. 869467. This output reflects only the author's view. The European Health and Digital Executive Agency (HaDEA) and the European Commission cannot be held responsible for any use that may be made of the information contained therein. J. López research was developed under the Margarita Salas postdoctoral fellowship from Ministerio de Universidades (MIU) and funded by the European Union-NextGeneration EU. Support for the research of J.L. Cortina was also received through the "ICREA Academia" recognition for excellence in research funded by the Generalitat de Catalunya.

Appendix A. Supplementary data

Supplementary data to this article can be found online at https://doi.org/10.1016/j.scitotenv.2024.171438.

References

Altıok, E., Şen, F., Wolska, J., Cyganowski, P., Bryjak, M., Kabay, N., Arda, M., Yüksel, M., 2023. Separation of boron and arsenic from geothermal water with novel gel-type chelating ion exchange resins: batch and column sorption-elution studies. Molecules 28, 7708. https://doi.org/10.3390/molecules28237708.

Bardi, U., 2010. Extracting minerals from seawater: an energy analysis. Sustainability 2, 980–992. https://doi.org/10.3390/su2040980.

Battaglia, G., Domina, M.A., Lo Brutto, R., Lopez Rodriguez, J., Fernandez de Labastida, M., Cortina, J.L., Pettignano, A., Cipollina, A., Tamburini, A., Micale, G., 2023. Evaluation of the purity of magnesium hydroxide recovered from saltwork bitterns. Water 15, 29. https://doi.org/10.3390/w15010029.

Bin Darwish, N., Kochkodan, V., Hilal, N., 2015. Boron removal from water with fractionized Amberlite IRA743 resin. Desalination 370, 1–6. https://doi.org/10.1016/j.desal.2015.05.009.

Bonin, L., Deduytsche, D., Wolthers, M., Flexer, V., Rabaey, K., 2021. Boron extraction using selective ion exchange resins enables effective magnesium recovery from lithium rich brines with minimal lithium loss. Sep. Purif. Technol. 275, 119177 https://doi.org/10.1016/j.seppur.2021.119177.

Burton, J., 2022. U.S. Geological Survey Releases 2022 List of Critical Minerals. U.S. Geological Survey. https://www.usgs.gov/news/national-news-release/us-geological-survey-releases-2022-list-critical-minerals. (Accessed 5 September 2023).

Çermikli, E., Şen, F., Altıok, E., Wolska, J., Cyganowski, P., Kabay, N., Bryjak, M., Arda, M., Yüksel, M., 2020. Performances of novel chelating ion exchange resins for boron and arsenic removal from saline geothermal water using adsorption-membrane filtration hybrid process. Desalination 491, 114504. https://doi.org/10.1016/j.desal.2020.114504.

Çermikli, E., Şen, F., Wolska, J., Cyganowski, P., Jarma, Y.A., Altıok, E., Arda, M., Bryjak, M., Kabay, N., 2023. Reclamation of reverse osmosis permeate and concentrate of geothermal water using novel chelating resins by hybrid method coupling adsorption and ultrafiltration. J. Membr. Sci. Res. 9, 559432 https://doi.org/10.22079/JMSR.2022.559432.1554.

CORDIS, 2021a. Development of Radical Innovations to Recover Minerals and Metals From Seawater Desalination Brines | Sea4Value Project. https://doi.org/10.3030/869703.

CORDIS, 2021b. Circular Processing of Seawater Brines From Saltworks for Recovery of Valuable Raw Materials | SEArcularMINE Project. https://doi.org/10.3030/869467.

Cyganowski, P., Şen, F., Altıok, E., Wolska, J., Bryjak, M., Kabay, N., Arda, M., Yüksel, M., 2021. Surface-activated chelating resins containing N-methyl-D-glucamine functional groups for desalination of geothermal water aimed for removal of boron and arsenic. Solvent Extr. Ion Exch. 39, 584–603. https://doi.org/10.1080/07366299.2021.1876385.

Davis, J.S., 2018. Structure, function and management of the biological system for seasonal solar saltworks. Global NEST J. 2, 217–226. https://doi.org/10.30955/gnj.000175.

European Commission, 2020. Study on the EU's List of Critical Raw Materials (2020) Final Report. https://doi.org/10.2873/11619.

European Commission, 2023. Critical Raw Materials | Internal Market, Industry, Entrepreneurship and SMEs. https://single-market-economy.ec.europa.eu/sectors/raw-materials/areas-specific-interest/critical-raw-materials_en. (Accessed 5 September 2023).

European Commission, Grohol, M., Veeh, C., 2023. Study on the Critical Raw Materials for the EU 2023 – Final Report. https://doi.org/10.2873/725585.

Figueira, M., Reig, M., Fernández de Labastida, M., Cortina, J.L., Valderrama, C., 2022. Boron recovery from desalination seawater brines by selective ion exchange resins. J. Environ. Manag. 314, 114984 https://doi.org/10.1016/j.jenvman.2022.114984.
Filingeri, A., Lopez, J., Culcasi, A., Leon, T., Tamburini, A., Luis Cortina, J., Micale, G., Cipollina, A., 2023. In-depth insights on multi-ionic transport in electrodialysis with bipolar membrane systems. Chem. Eng. J. 468 https://doi.org/10.1016/j.cej.2023.143673, 143673 Contents.
Gorjian, S., Jamshidian, F.J., Hosseinqolilou, B., 2019. Feasible solar applications for brines disposal in desalination plants. In: Kumar, A., Prakash, O. (Eds.), Solar Desalination Technology. Springer, Singapore, pp. 25–48. https://doi.org/10.1007/978-981-13-6887-5.
Guan, Z., Lv, J., Bai, P., Guo, X., 2016. Boron removal from aqueous solutions by adsorption - a review. Desalination 383, 29–37. https://doi.org/10.1016/j.desal.2015.12.026.
Hubicki, Z., Kołodyńska, D., 2012. Chapter 8 - selective removal of heavy metal ions from waters and waste waters using ion exchange methods. In: Ion Exchange Technologies, pp. 193–240. https://doi.org/10.5772/51040.
Ipek, I.Y., Kabay, N., Yuksel, M., Kirmizisakal, O., Bryjak, M., 2009. Removal of boron from Balçova-Izmir geothermal water by ion exchange process: batch and column studies. Chem. Eng. Commun. 196, 277–289. https://doi.org/10.1080/00986440802289971.
Jeppesen, T., Shu, L., Keir, G., Jegatheesan, V., 2009. Metal recovery from reverse osmosis concentrate. J. Clean. Prod. 17, 703–707. https://doi.org/10.1016/j.jclepro.2008.11.013.
Jung, S., Kim, M.-J., 2016. Optimal conditions for recovering boron from seawater using boron selective resins. Korean J. Chem. Eng. 33, 2411–2417. https://doi.org/10.1007/s11814-016-0096-4.
Kabay, N., Sarp, S., Yuksel, M., Arar, Ö., Bryjak, M., 2007. Removal of boron from seawater by selective ion exchange resins. React. Funct. Polym. 67, 1643–1650. https://doi.org/10.1016/j.reactfunctpolym.2007.07.033.
Kabay, N., Güler, E., Bryjak, M., 2010. Boron in seawater and methods for its separation - a review. Desalination 261, 212–217. https://doi.org/10.1016/j.desal.2010.05.033.
Kumar, A., Naidu, G., Fukuda, H., Du, F., Vigneswaran, S., Drioli, E., Lienhard, J.H., 2021. Metals recovery from seawater desalination brines: technologies, opportunities, and challenges. ACS Sustain. Chem. Eng. 9, 7704–7712. https://doi.org/10.1021/acssuschemeng.1c00785.
León, T., Abdullah Shah, S., López, J., Culcasi, A., Jofre, L., Cipollina, A., Cortina, J.L., Tamburini, A., Micale, G., 2022. Electrodialysis with bipolar membranes for the generation of NaOH and HCl solutions from brines: an inter-laboratory evaluation of thin and ultrathin non-woven cloth-based ion-exchange membranes. Membranes 12, 1204. https://doi.org/10.3390/membranes12121204.
Loganathan, P., Naidu, G., Vigneswaran, S., 2017. Mining valuable minerals from seawater: a critical review. Environ. Sci.: Water Res. Technol. 3, 37–53. https://doi.org/10.1039/c6ew00268d.
Louati, I., Guesmi, F., Chaabouni, A., Hannachi, C., Hamrouni, B., 2016. Effect of ionic strength on the ion exchange equilibrium between AMX membrane and electrolyte solutions. Water Qual. Res. J. Can. 51, 60–68. https://doi.org/10.2166/wqrjc.2015.006.
Maskal, J., Thompson, I.M., Waldron, G.W., 1966. US3447899A-Method of Purifying Magnesium Values.
Mazur, L.P., Pozdniakova, T.A., Mayer, D.A., de Souza, S.M.A.G.U., Boaventura, R.A.R., Vilar, V.J.P., 2017. Cation exchange prediction model for copper binding onto raw brown marine macro-algae Ascophyllum nodosum: batch and fixed-bed studies. Chem. Eng. J. 316, 255–276. https://doi.org/10.1016/j.cej.2017.01.080.
Melnyk, L., Goncharuk, V., Butnyk, I., Tsapiuk, E., 2005. Boron removal from natural and wastewaters using combined sorption/membrane process. Desalination 185, 147–157. https://doi.org/10.1016/j.desal.2005.02.076.
Mestri, S., Dogan, S., Tizaoui, C., 2023. Bromate removal from water using ion exchange resin: batch and fixed bed column performance, ozone. Sci. Eng. 45, 291–304. https://doi.org/10.1080/01919512.2022.2114420.
Mitsubishi Chemical, 2007. Diaion CRB03 Product Data Sheet.
Mitsubishi Chemical, 2011. Diaion CRB05 Product Data Sheet.
Nasef, M.M., Nallappan, M., Ujang, Z., 2014. Polymer-based chelating adsorbents for the selective removal of boron from water and wastewater: a review. React. Funct. Polym. 85, 54–68. https://doi.org/10.1016/j.reactfunctpolym.2014.10.007.
Nishihama, S., Sumiyoshi, Y., Ookubo, T., Yoshizuka, K., 2013. Adsorption of boron using glucamine-based chelate adsorbents. Desalination 310, 81–86. https://doi.org/10.1016/j.desal.2012.06.021.
Pramanik, B.K., Nghiem, L.D., Hai, F.I., 2020. Extraction of strategically important elements from brines: constraints and opportunities. Water Res. 168, 115149 https://doi.org/10.1016/j.watres.2019.115149.
Purolite, 2020. Purolite S108 Product Data Sheet, S108 Product Data Sheet.
Quist-Jensen, C.A., Macedonio, F., Drioli, E., 2016. Membrane crystallization for salts recovery from brine—an experimental and theoretical analysis. Desalin. Water Treat. 57, 7593–7603. https://doi.org/10.1080/19443994.2015.1030110.
Randazzo, S., Vicari, F., López, J., Salem, M., Lo Brutto, R., Azzouz, S., Chamam, S., Cataldo, S., Muratore, N., Fernández de Labastida, M., Vallès, V., Pettignano, A., Staiti, G.D., Pawlowski, S., Hannachi, A., Cortina, J.L., Cipollina, A., 2024. Unlocking hidden mineral resources: characterization and potential of bitterns as alternative sources for minerals in Mediterranean Saltworks. J. Clean. Prod. 436, 140412 https://doi.org/10.1016/j.jclepro.2023.140412.
Reig, M., Vecino, X., Hermassi, M., Valderrama, C., Gibert, O., Cortina, J.L., 2019. Integration of selectrodialysis and solvent-impregnated resins for Zn(II) and Cu(II) recovery from hydrometallurgy effluents containing As(V). Sep. Purif. Technol. 229, 115818 https://doi.org/10.1016/j.seppur.2019.115818.
Robinson, H.A., Friedrich, R.E., Spencer, R.S., 1943. US2405055-Magnesium Hydroxide From Seawater, 492860.
Romano, S., Trespi, S., Achermann, R., Battaglia, G., Raponi, A., Marchisio, D., Mazzotti, M., Micale, G., Cipollina, A., 2023. The role of operating conditions in the precipitation of magnesium hydroxide hexagonal platelets using NaOH solutions. Cryst. Growth Des. 23, 6491–6505. https://doi.org/10.1021/acs.cgd.3c00462.
Saif, H.M., Huertas, R.M., Pawlowski, S., Crespo, J.G., Velizarov, S., 2021. Development of highly selective composite polymeric membranes for Li+/Mg2+ separation. J. Membr. Sci. 620, 118891 https://doi.org/10.1016/j.memsci.2020.118891.
Saif, H.M., Crespo, J.G., Pawlowski, S., 2023. Lithium recovery from brines by lithium membrane flow capacitive deionization (Li-MFCDI) – a proof of concept. J. Membr. Sci. Lett. 3, 100059 https://doi.org/10.1016/j.memlet.2023.100059.
SEArcularMINE, 2020. Circular Processing of Seawater Brines from Saltworks for Recovery of Valuable Raw Materials - SEArcularMINE. https://searcularmine.eu/. (Accessed 9 May 2021).
Şen, F., Altıok, E., Cyganowski, P., Wolska, J., Bryjak, M., Kabay, N., Arda, M., Yüksel, M., 2021. Reclamation of RO permeate and concentrate of geothermal water by new chelating resins having N-methyl-D-glucamine ligands. Sep. Purif. Technol. 254, 117558 https://doi.org/10.1016/j.seppur.2020.117558.
Shahmansouri, A., Min, J., Jin, L., Bellona, C., 2015. Feasibility of extracting valuable minerals from desalination concentrate: a comprehensive literature review. J. Clean. Prod. 100, 4–16. https://doi.org/10.1016/j.jclepro.2015.03.031.
Shao, L., Sheng, C., Lu, M., Yang, Y., Li, P., 2023. Boron continuous recovery from brines by the multicolumn simulated moving bed process with boron chelating resin. J. Water Process Eng. 53 https://doi.org/10.1016/j.jwpe.2023.103875.
Sharkh, B.A., Al-Amoudi, A.A., Farooque, M., Fellows, C.M., Ihm, S., Lee, S., Li, S., Voutchkov, N., 2022. Seawater desalination concentrate—a new frontier for sustainable mining of valuable minerals. Npj Clean Water 5, 9. https://doi.org/10.1038/s41545-022-00153-6.
Simonnot, M.-O., Castel, C., Nicolaï, M., Rosin, C., Sardin, M., Jauffret, H., 2000. Boron removal from drinking water with a boron selective resin: is the treatment really selective? Water Res. 34, 109–116. https://doi.org/10.1016/S0043-1354(99)00130-X.
Thabit, Q., Nassour, A., Nelles, M., 2022. Water desalination using the once-through multi-stage flash concept: design and modeling. Materials 15, 6131. https://doi.org/10.3390/ma15176131.
Vallès, V., López, J., Fernández de Labastida, M., Gibert, O., Leskinen, A., Koivula, R.T., Cortina, J.L., 2023a. Polymeric and inorganic sorbents as a green option to recover critical raw materials at trace levels from sea saltwork bitterns. Green Chem. 700–719. https://doi.org/10.1039/d2gc02338e.
Vallès, V., Fernández de Labastida, M., López, J., Battaglia, G., Winter, D., Randazzo, S., Cipollina, A., Cortina, J.L., 2023b. Sustainable recovery of critical elements from seawater saltworks bitterns by integration of high selective sorbents and reactive precipitation and crystallisation: developing the probe of concept with on-site produced chemicals and energy. Sep. Purif. Technol. 306, 122622 https://doi.org/10.1016/j.seppur.2022.122622.
Vassallo, F., La Corte, D., Cancilla, N., Tamburini, A., Bevacqua, M., Cipollina, A., Micale, G., 2021. A pilot-plant for the selective recovery of magnesium and calcium from waste brines. Desalination 517, 115231. https://doi.org/10.1016/j.desal.2021.115231.
Vicari, F., Randazzo, S., López, J., de Labastida, M.F., Vallès, V., Micale, G., Tamburini, A., Staiti, G.D., Cortina, J.L., Cipollina, A., Fernández de Labastida, M., Vallès, V., Micale, G., Tamburini, A., D'Alì Staiti, G., Cortina, J.L., Cipollina, A., 2022. Mining minerals and critical raw materials from bittern: understanding metal ions fate in saltwork ponds. Sci. Total Environ. 847 https://doi.org/10.1016/j.scitotenv.2022.157544.
Virolainen, S., Heinonen, J., Paatero, E., 2013. Selective recovery of germanium with N-methylglucamine functional resin from sulfate solutions. Sep. Purif. Technol. 104, 193–199. https://doi.org/10.1016/j.seppur.2012.11.023.
Wen, Z., Yao, Y., Niu, Y., Zhou, G., Xu, G., Zhong, H., 2016. Adsorption mechanism of weakly basic anion exchange resin for uranium in acidic leaching solution containing uranium. Zhongnan Daxue Xuebao (Ziran Kexue Ban)/J. Central South Univ. (Sci. Technol.) 47, 1867–1871. https://doi.org/10.11817/j.issn.1672-7207.2016.06.007.
Wolska, J., Bryjak, M., 2013. Methods for boron removal from aqueous solutions — a review. Desalination 310, 18–24. https://doi.org/10.1016/j.desal.2012.08.003.
Zhang, X., Zhao, W., Zhang, Y., Jegatheesan, V., 2021. A review of resource recovery from seawater desalination brine. Rev. Environ. Sci. Biotechnol. 20, 333–361. https://doi.org/10.1007/s11157-021-09570-4.